A dual domain decomposition method for finite element digital image correlation

Jean-Charles Passieux, Jean-Noël Périé, Michel Salaün

International Journal for Numerical Methods in Engineering
Accepted 2015, doi: 10.1002/nme.4868

A dual domain decomposition method for finite element digital image correlation

J.-C. Passieux J.-N. Périé and M. Salaün

Université de Toulouse, Institut Clément Ader (ICA) FRE CNRS 3687, INSA Toulouse/UPS/ISAE/Mines Albi, 3 rue Caroline Aigle, 31400 Toulouse, France

Abstract The computational burden associated to finite element based digital image correlation methods is mostly due to the inversion of finite element systems and to image interpolations. A non-overlapping dual domain decomposition method is here proposed to rationalize the computational cost of high resolution finite element digital image correlation measurements when dealing with large images. It consists in splitting the global mesh into submeshes and the reference and deformed states images into subset images. Classic finite element digital image correlation formulations are first written in each subdomain independently. The displacement continuity at the interfaces is enforced by introducing a set of Lagrange multipliers. The problem is then condensed on the interface and solved by a conjuguate gradient algorithm. Three different preconditionners are proposed to accelerate its convergence. The proposed domain decomposition method is here exemplified with real high resolution images. It is shown to combine the metrological performances of finite element based digital image correlation and the parallelisation ability of subset based methods.

keywords parallel computing, global DIC, high performance computing, substructuring, finite elements, domain decomposition

1 Introduction

The analysis of the mechanical behavior of materials and structures rely more and more on full-field measurements. It is mainly due the large quantity of data they provide, which are particularly interesting for parameter identification purposes for instance. Among them, Digital Image Correlation (DIC) has become one of the most popular because of a favorable ease of use to accuracy ratio [46, 45] and its ability to deal with 3D measurements on the surface (stereo DIC [27]) and also in the bulk with Digital Volume Correlation (DVC [1, 37]). In continuum solid mechanics, finite element based DIC (FE-DIC [44, 3, 11, 17]) has proved to be a relevant choice since (a) it allows for interpolation-free communications with finite element simulations, (b) it significantly reduces the measurement uncertainties with respect to classical subset based approaches [17], since prescribed continuity of the unknown displacement fields acts as a regularisation. The drawback of FE-DIC over subset-DIC [45] is the computational cost when high resolution is sought for [24, 35]. Indeed, subset based DIC approaches lead to a set of small independent nonlinear systems of equations which are highly parallelisable, whereas FE-DIC method lead to one global non-linear system whose inversion can become prohibitive with a large number of degrees of freedom [35]. In addition, due to the constantly increasing resolution of photographic sensors (standard sensors provide nowadays 29 million pixels, which can be extended up to 260 million pixels using a piezoelectric pixel shift), the manipulation and interpolation of images (large dense matrices) become more and more an issue. This problem is even more acute with tomographic images.

The two main causes responsible for the high computational cost of high resolution FE-DIC are thus system inversions and image interpolations. A method that addresses the first issue consists in reducing the dimensionnality of the problem. A variable separation technique based on the Proper Generalised Decomposition (PGD) has been proposed recently to decrease the numerical complexity of FE-DIC [35, 13], while preserving the above mentioned advantages. It was shown that it may drastically reduce the computation time associated to the resolution of the FE systems. Another attempt based on GPU implementation proposed recently to adress both sources of computational cost [22]. However, the limitations remain when the size of the region of interest increases.

In the community of numerical simulation, a family of solvers, referred to as *domain decomposition methods* (DDM) has been developed for high performance computing on parallel computer architectures. The domain decomposition methods, such as Schwarz methods [12], were originally based on overlapping partitions of the studied region. Then non-overlapping methods were preferred because of their ease of implementation. The dual domain decomposition (such as Finite Element Tearing and Interconnecting, FETI [9]) seeks iteratively the displacement continuity at the interface assuming the equilibrium of the subdomains. On the contrary, primal domain decomposition methods (such as Balancing Domain Decomposition, BDD [28]) prescribe displacement continuity and get iteratively equilibrium at the interface. Mixed [21, 43, 33] and hybrid [14] alternatives have also been proposed that mixes primal and dual approaches. Most often, the global problem is condensed onto the interface degrees of freedom and solved by a Krylov iterative algorithm [9, 28]. The latter can be computed in parallel since it involves independent problems on each subdomain.

In the same way, a dual non-overlapping domain decomposition algorithm is proposed herein, in the context of FE-DIC, to alleviate both finite element system solving and image manipulation issues at the same time. The method consists in splitting the domain into a set of subdomains (with submeshes and subset images). The algorithm based on the preconditionned conjugate gradient thus involves a set of smaller independent problems (based on small meshes and small subset images) well suited for parallel processing. Three different preconditionners are proposed with different extra-costs and efficiencies. After describing its principle, the method is used to analyse high resolution images of a real experiment.

2 The proposed domain decomposition approach

2.1 Digital image correlation

Let us consider two grayscale images $f(\mathbf{x})$ and after $g(\mathbf{x})$ corresponding to the reference and deformed states of the specimen respectively. The displacement field between those two states is denoted $\mathbf{u}(\mathbf{x})$, where $\mathbf{x} \in \Omega$ is a point in the region of interest Ω of the image. Given f and g, the DIC problem consists in finding the displacement field $\mathbf{u}^\star \in \mathbf{L}^2(\Omega)$ (where $\mathbf{L}^2(\Omega)$ defines Hilbert space $[L^2(\Omega)]^d$ with $d = 2$ for DIC and 3 for DVC) that best fullfils the graylevel conservation equation [19]:

$$\mathbf{u}^\star = \underset{\mathbf{u}(\mathbf{x})\in\mathbf{L}^2(\Omega)}{\arg\min} \int_\Omega \Big(f(\mathbf{x}) - g(\mathbf{x}+\mathbf{u}(\mathbf{x}))\Big)^2 d\mathbf{x} \tag{1}$$

Problem (1) is nonlinear. Assuming that g (and thus f) is differentiable, it can be solved by a Newton-like algorithm. At iteration k the unknown displacement correction $\delta\mathbf{u}^k = \mathbf{u}^k - \mathbf{u}^{k-1}$ is assumed to be small enough to allow for a first order Taylor expansion of the deformed state image

$$g(\mathbf{x}+\mathbf{u}^k) \approx g(\mathbf{x}+\mathbf{u}^{k-1}) + \delta\mathbf{u}^{k^T} \nabla g(\mathbf{x}+\mathbf{u}^{k-1}) \tag{2}$$

In equation (2), $\nabla g(\mathbf{x}+\mathbf{u}^{k-1})$ denotes the gradient of image g at non integer pixels positions $\mathbf{x}+\mathbf{u}^{k-1}$. Since $g(\mathbf{x}+\mathbf{u}^{k-1})$ is supposed to converge to $f(\mathbf{x})$, the gradient $\nabla g(\mathbf{x}+\mathbf{u}^{k-1})$ is approximated by $\nabla f(\mathbf{x})$, which does not depend on the unknown and which can then be computed once and for all.

The stationnarity conditions associated to the minimisation of the linearised version of Problem (1) yields the following variationnal formulation:

$$a(\delta\mathbf{u}^k, \mathbf{v}) = l^k(\mathbf{v}) \qquad \forall \mathbf{v} \in \mathbf{L}^2(\Omega) \tag{3}$$

where $\forall(\mathbf{u},\mathbf{v}) \in \mathbf{L}^2(\Omega)\times\mathbf{L}^2(\Omega)$,

$$a(\mathbf{u},\mathbf{v}) = \int_\Omega \mathbf{v}^T \nabla f \, \nabla f^T \mathbf{u} \, d\mathbf{x} \quad \text{and} \quad l^k(\mathbf{v}) = \int_\Omega \mathbf{v}^T \nabla f \, \big(f(\mathbf{x}) - g(\mathbf{x}+\mathbf{u}^{k-1})\big) \, d\mathbf{x}$$

As such, this problem is ill-posed in Hadamar's sense, *i.e.* the displacement cannot be found pixel-wise. This problem needs to be regularised. For that the unknown displacement $\mathbf{u}(\mathbf{x})$ is searched for in an approximation subspace $\mathcal{V} \subset \mathbf{L}^2(\Omega)$ whose dimension is much smaller than the number of pixels in Ω. Generally, $\mathcal{V}$ is defined by a set of basis functions $\mathbf{N}_i(\mathbf{x})$. The approximation of the displacement thus reads $\delta\mathbf{u}^k(\mathbf{x}) = \sum_i \mathbf{N}_i(\mathbf{x})\, q_i^k$ where q_i^k are the corresponding coefficients of the linear combination, referred to as degrees of freedom (dof) of the displacement correction at iteration k.

By applying the Galerkin method, Problem (3) produces, at iteration k, the following linear system of equations:

$$\mathbf{M}\,\mathbf{q}^k = \mathbf{b}^k \tag{4}$$

where $\mathbf{q}^k$ is a vector collecting the dof q_i^k and

$$\mathbf{M}_{ij} = a(\mathbf{N}_i(\mathbf{x}), \mathbf{N}_j(\mathbf{x})) \qquad \text{and} \qquad \mathbf{b}_j^k = l^k(\mathbf{N}_j(\mathbf{x})) \tag{5}$$

The correlation operator $\mathbf{M}$ is symmetric positive definite [10].

The choice of the approximation subspace $\mathcal{V}$ or more precisely of its basis functions $\mathbf{N}_i(\mathbf{x})$ may be varied: piecewise constant [26] or polynomial functions [46], Fourier series [42, 30], rigid body translations and rotations [32, 34], B-splines [6, 8], NURBS [7], finite elements [44, 3, 11], eXtended finite elements [40, 37], separation of variable [35, 13], mechanical [41, 18, 4] and optical analytical function [39] or numerical precomputed functions [23].

As regards computational costs, the *so-called* subset methods, that rely on piecewise polynomial functions, involve a bloc diagonal correlation operator $\mathbf{M}$. Its resolution is therefore highly parallelisable. In opposition, with almost all the other interpolation types, and in particular with finite elements, the operator $\mathbf{M}$ is global. Its size, which is equal to the dimension of the approximation subspace (or the number of dofs), can become prohibitive when high resolution is required [24, 35, 13].

As stated in the introduction, the second main computational limitations, which is not peculiar to FE-DIC, is the computation of the right hand side $\mathbf{b}^k$. The latter needs to evaluate the deformed state image g at the non-integer pixels values $\mathbf{x} + \mathbf{u}^{k-1}(\mathbf{x})$. This implies using interpolation algorithms whose computational complexity scales in $\mathcal{O}(n\ log(n))$ where n is the number of points.

The computational cost of FE-DIC may become significant when high resolution images and meshes are jointly used. In the following, a domain decomposition algorithm is proposed to alleviate both computational issues associated to the resolution of large systems and the manipulation of large images.

Remark. The subset based approaches [26, 46] could be seen as a kind of overlapping partition of the region of interest since the size of the step between two subsets can be set smaller than the size of the subset itself. However, all the problems on the subsets are solved independently and the displacement continuity across interfaces is not searched for.

2.2 Domain decomposition

Let us now consider a non-overlapping partition of the region of interest Ω into a set of subdomains Ω_s. In the same way any quantity with subscript $\square_s$ defines the restriction to Ω_s of quantity $\square$. For the sake of simplicity, the method will be first presented in the case of two subdomains Ω_1 and Ω_2 without loss of generality. In each subdomain, the linearised correlation problem at iteration k reads: find $\delta\mathbf{u}_s^k \in \mathbf{L}^2(\Omega_s)$, such that

$$\forall s, \forall \mathbf{v}_s \in \mathbf{L}^2(\Omega_s), \qquad a_s(\delta\mathbf{u}_s^k, \mathbf{v}_s) = l_s^k(\mathbf{v}_s) \tag{6}$$

Problem (6) must be solved under the constraint of displacement continuity at the interface $\Gamma = \Omega_1 \cap \Omega_2$, see Figure 1. For that a Lagrange multiplier $\lambda \in \mathcal{L}$ ($\mathcal{L}$ being the *ad-hoc* space) is introduced to ensure this constraint in a weak sense:

$$\langle \mathbf{u}_1 - \mathbf{u}_2, \lambda \rangle = \lambda^T\ (\mathbf{u}_1|_\Gamma - \mathbf{u}_2|_\Gamma) = 0 \tag{7}$$

The three fields formulation thus reads, $\forall (\mathbf{v}_1, \mathbf{v}_2, \mu) \in \mathbf{L}^2(\Omega_1) \times \mathbf{L}^2(\Omega_2) \times \mathcal{L}$,

$$\begin{aligned} a_1(\delta\mathbf{u}_1^k, \mathbf{v}_1) + a_2(\delta\mathbf{u}_2^k, \mathbf{v}_2) + \langle \delta\mathbf{u}_1^k - \delta\mathbf{u}_2^k, \mu \rangle + \langle \mathbf{v}_1 - \mathbf{v}_2, \lambda \rangle & \\ = l_1^k(\mathbf{v}_1) + l_2^k(\mathbf{v}_2) + \langle \mathbf{u}_2^{k-1} - \mathbf{u}_1^{k-1}, \mu \rangle & \end{aligned} \tag{8}$$

When introduced in formulation (8), the finite element interpolation leads to the following coupled linear system:

$$\begin{bmatrix} \mathbf{M}_1 & 0 & \mathbf{C}_1^T \\ 0 & \mathbf{M}_2 & \mathbf{C}_2^T \\ \mathbf{C}_1 & \mathbf{C}_2 & 0 \end{bmatrix} \begin{bmatrix} \mathbf{q}_1^k \\ \mathbf{q}_2^k \\ \mathbf{\Lambda} \end{bmatrix} = \begin{bmatrix} \mathbf{b}_1^k \\ \mathbf{b}_2^k \\ -\mathbf{C}_1\mathbf{p}_1 - \mathbf{C}_2\mathbf{p}_2 \end{bmatrix} \tag{9}$$

where $\mathbf{\Lambda}$, $\mathbf{p}_1$ and $\mathbf{p}_2$ are the dof vectors corresponding to the FE interpolation of λ, $\mathbf{u}_1^{k-1}$ and $\mathbf{u}_2^{k-1}$ respectively. $\mathbf{C}_s$ denote rectangular signed boolean operators such that if a dof belong to Γ, his value is set to 1 and the corresponding dof on the other side of Γ is set to -1.

As such, Problem (9) is coupled and involves all the unknown and the data of the image in the entire region of interest Ω. It is thus obviously not solved directly. In order to rationalize the computational cost of FE-DIC, the problem is split into the following coupled equations:

$$\mathbf{q}_s^k = \mathbf{M}_s^{-1}(\mathbf{b}_s^k - \mathbf{C}_s^T\mathbf{\Lambda}) \qquad \forall s \tag{10}$$

$$\sum_s \mathbf{C}_s \left(\mathbf{q}_s^k + \mathbf{p}_s\right) = 0 \tag{11}$$

The dual interface problem is then obtained by the condensation of Problem (9) on Interface Γ. It consists in substituting equations (10) into equation (11):

$$\mathbf{S}^d \, \mathbf{\Lambda} = \mathbf{t}^k \tag{12}$$

where the condensed right hand side $\mathbf{t}^k$ and the *so-called* dual Shur complement operator $\mathbf{S}^d$ read

$$\mathbf{S}^d = \sum_s \mathbf{C}_s \mathbf{M}_s^{-1} \mathbf{C}_s^T \tag{13}$$

$$\mathbf{t}^k = \sum_s \mathbf{C}_s \left(\mathbf{p}_s + \mathbf{M}_s^{-1} \mathbf{b}_s^k \right) \tag{14}$$

Remark. It is easy to see that Problem (12) remains in the same form when more than two subdomains are considered. Nevertheless, attention must be paid to the interface dof belonging to more than two subdomains (multiplicity greater than 2). If an interface node is linked to n subdomains, $n-1$ Lagrange multipliers are introduced in each dimension.

2.3 Iterative solution algorithm

Introducing a decomposition of the domain and writing the condensed problem at the interface is not sufficient to make this method parallelisable. More, operator $\mathbf{S}^d$ is formally based on the inversion of the local correlation operators $\mathbf{M}_s$ whose computation cost would be prohibitive. Obviously, it is actually neither computed nor assembled. Indeed, the condensed symmetric linear system (12) is solved thanks to a preconditionned conjugate gradient (CG) solver. After initialisation $\mathbf{r}_0 = \mathbf{t}^k - \mathbf{S}^d \mathbf{\Lambda}_0$ and $\mathbf{d}_0 = \mathbf{P}^{-1} \mathbf{r}_0$, one iteration of the preconditionned CG reads:

$$\alpha = \frac{\mathbf{r}_i^T \mathbf{P}^{-1} \mathbf{r}_i}{\mathbf{d}_i^T \mathbf{S}^d \mathbf{d}_i} \tag{15}$$

$$\mathbf{\Lambda}_{i+1} = \mathbf{\Lambda}_i + \alpha \, \mathbf{d}_i \tag{16}$$

$$\mathbf{r}_{i+1} = \mathbf{r}_i - \alpha \, \mathbf{S}^d \mathbf{d}_i \tag{17}$$

$$\beta = \frac{\mathbf{r}_{i+1}^T \mathbf{P}^{-1} \mathbf{r}_{i+1}}{\mathbf{r}_i^T \mathbf{P}^{-1} \mathbf{r}_i} \tag{18}$$

$$\mathbf{d}_{i+1} = \mathbf{P}^{-1} \mathbf{r}_{i+1} + \beta \, \mathbf{d}_i \tag{19}$$

where $\mathbf{P}$ is a preconditionner whose choice is discussed later. As written in the above algorithm, the conjugate gradient only requires matrix-vector products between operator $\mathbf{S}^d$ and vector $\mathbf{d}_i$. As $\mathbf{S}^d$ is expressed as a sum on subdomains, this product corresponds to the following computation:

$$\mathbf{S}^d \mathbf{d}_i = \sum_s \mathbf{C}_s \mathbf{M}_s^{-1} \mathbf{C}_s^T \mathbf{d}_i = \sum_s \mathbf{C}_s \mathbf{y}_s$$

where $\mathbf{y}_s$ are the solutions of the set of local systems $\mathbf{M}_s \mathbf{y}_s = \mathbf{C}_s^T \mathbf{d}_i$ that correspond to local correlation problems with different right hand sides. These system inversions are thus computationally affordable and, above all, independent from one subdomain to the other. That means that parallel processing can be used when computing these local products. Since the right hand side $\mathbf{t}^k$ is the sum of local contributions $\mathbf{t}_s^k$, it can also be computed in parallel. Note that operators $\mathbf{M}_s$ remains unchanged during correlation iterations k. They can be factorised once at the beginning. The stopping criterion of the CG is classically based on the norm of the residual $\mathbf{r}_{i+1}$.

The resulting domain decomposition DIC method yields exacly the solution one would get with one single mesh and a classical FE-DIC. The metrological performances of this method are thus the same than a classical FE-DIC method with a unique subdomain [17].

2.4 Image decomposition

However, as stated earlier, the computation of the local contributions to the left and right hand side of (12) requires to manipulate and interpolate images f and g at non-interger pixels positions within subdomain Ω_s. In order to reduce the computational burden associated to whole image interpolation, we propose also to subdivide images f and g in a set of rectangular subset images f_s and g_s surrounding domain Ω_s as it is usually done in subset-based approaches [45]. More precisely, g_s is interpolated at the position $\mathbf{x} + \mathbf{u}(\mathbf{x})$. Since $\mathbf{u}$ is neither constant within subdomain Ω_s nor zero mean, g_s is defined up to the average rigid body translation estimated

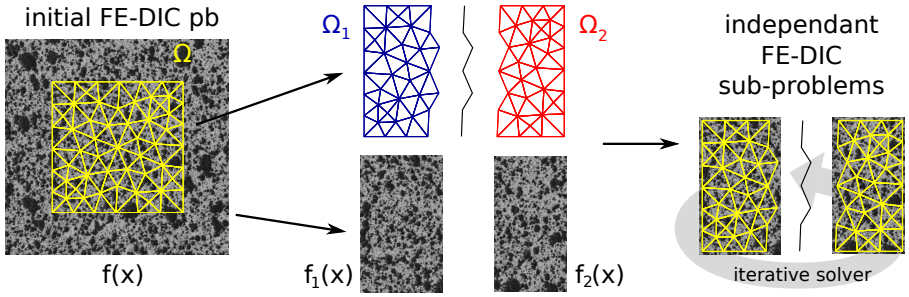

Figure 1: Global image f and domain Ω decomposition in two subdomains Ω_s and two subset images f_s. A set of subset of image g are also built. Note that subdomains and submeshes are not overlapping, but subset images are.

by a Fast Fourier Transform, and it is a bit larger than f_s. As in subset based methods, it may appear that the displacement $\mathbf{u}_s$ is such that $\mathbf{x} + \mathbf{u}_s$ is larger than initially estimated subset image g_s. A simple test is done before each interpolation step in order to avoid such a problem by enlarging or shifting the corresponding deformed subset image g_s.

Therefore the computational effort associated to both finite elements (system inversions) and image interpolations are local, and thus parallelisable. A scheme of the image and mesh decomposition is provided in Figure 1. Not only these computations can be made on parallel computers, but the complexity and memory requirements of both system inversion and image interpolation are such that this method may be of interest in the context of high resolution analyses even in a sequential implementation.

2.5 Initialisation

Initialisation of the DIC iterations. Since a Newton-like solver is used for solving the correlation problem, a good initial value $\mathbf{u}^0(\mathbf{x})$ of the unknwon displacement is required. In practice, the algorithm is here initialised by the solution to DIC problems in each subdomain independently. These problems correspond to classical FE-DIC analyses performed independently on each subdomain. Note that these problems may themselves be also initialised by multigrid and coarse graining techniques [16, 13] in order to avoid local minimas. This provides a good initial estimate of the unknown displacement as shown in the examples below. The displacement of the inner nodes in the subdomains are almost converged. The correction computed by the proposed domain decomposition method mostly concerns nodes near the interface. Therefore, only a few extra iterations on the correlation problem are required using the proposed domain decomposition method, to bond the subdomains solutions.

Initialisation of the CG iterations. One conjugate gradient solver is used at each correlation iteration k. Each time, an initial value of $\mathbf{\Lambda}$ is also required. In practice, the first one (iteration $k = 0$) is set to zero, and the next ones ($k > 0$) are set to the last value of the previous CG resolution. This is a very naive but effective way to reduce the number of CG iterations, as shown in the examples below.

2.6 Convergence acceleration

In addition to a good initialisation, there are obviously many more efficient ways to speed-up a CG resolution. For instance, one can use preconditionning [12, 9]. The idea is to improve the condition number of the initial operator $\mathbf{S}^d$ on which depend the convergence rate of the CG. In practice, a classical choice consists in constructing an operator $\mathbf{P}$ that is an approximation of $\mathbf{S}^d$ but easier to invert. The preconditionned conjuguate gradient solver (15-19) consists in solving the problem $\mathbf{P}^{-1}\mathbf{S}^d\mathbf{\Lambda} = \mathbf{P}^{-1}\mathbf{t}_s^k$. In the following, we propose to use three basic preconditionners, listed in an increasing order of efficiency:

1. the *double diagonal* preconditionner which is both cheap to build and to use in the preconditionned conjugate gradient (PCG), since the resulting operator is diagonal:

$$\mathbf{P}_{dd} = \sum_s diag(\mathbf{C}_s \; diag(\mathbf{M}_s)^{-1}\mathbf{C}_s^T)$$

2. the *diagonal* preconditionner which is a bit more expensive to assemble since local operators $\mathbf{M}_s$ need to be inverted. Its cost is however affordable since it has to be done once and comparable to the cost of the

so-called Dirichlet preconditionner of FETI [9]:

$$\mathbf{P}_d = \sum_s diag(\mathbf{C}_s\ \mathbf{M}_s^{-1}\mathbf{C}_s^T)$$

3. the *quasi-diagonal* preconditionner. Its assembly is almost as cheap as the *double diagonal*, but it is not exactly diagonal.

$$\mathbf{P}_{qd} = \sum_s \mathbf{C}_s\ diag(\mathbf{M}_s)^{-1}\mathbf{C}_s^T$$

In practice, $\mathbf{C}_s\mathbf{C}_s^T$ are band matrices and their bandwidth, *a priori*, depends on the numbering of the Lagrange multipliers and the dimension of the problem (2D in this case). However, it is possible to build a tridiagonal operator by using an appropriate numbering of the Lagrange multipliers. Two rules have to be considered: (1) an interface dof in one subdomain must not be associated to more than 2 Lagrange multipliers (which is possible even for multiplicity higher than 2) and (2) the Lagrange multipliers must be sorted by physical dimension (first x dofs, then y dofs). It can be noticed that such a method will also work in 3D DVC. Furthermore, the number of non-zero extra diagonal values is equal to the sum of the multiplicity of each interface dof minus the number of interface dof, which, at least in 2D DIC, is very low. However, it is necessary to perform a Cholesky factorisation, for instance, once and for all the correlation iterations. Then, at each CG iteration, a forward and a backward substitution is performed. The associated extra cost is therefore very reasonable.

Remarks Another possibility would consists in computing a lumped correlation operator as what is done in transient dynamics [2]. But according to our tests, and thanks to the short varying evolution of the image gradients, our implementation of such a technique was not efficient for preconditionning a domain-decomposition DIC problem. Beyond preconditionning, another way to accelerate the CG resolution would be to reuse Krylov subspaces [15] which would be particularly efficient in this case since the operator is constant and the right hand side changes little.

Finally, a scheme of the domain decomposition DIC algorithm is given in Figure 2.

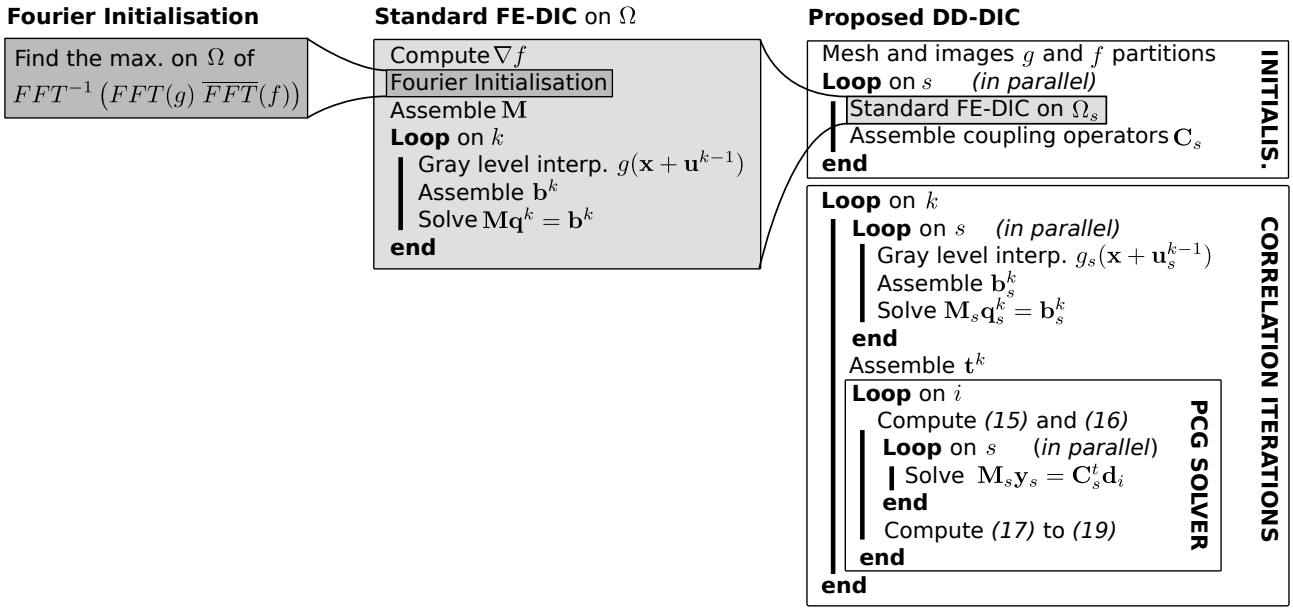

Figure 2: A scheme highlighting the link between the proposed approach, the conventional FE-DIC strategy and piecewise constant Fourier based approach used for initialisation.

3 Application to a four point bending test

3.1 Experimental setup

The domain decomposition method previously described is now applied to the analysis of a four point bending test performed on an open hole polymethyl methacrylate (PMMA) specimen. The latter is a parallelepipedic

coupon of dimension $200 \times 20 \times 5$mm with a 8mm hole drilled in the center. A black and white speckle pattern is sprayed onto the surface of the specimen. A high resolution CCD camera (29 megapixels) has been used to capture images (4384×6576 pixels). An unstructured finite element mesh (including both linear triangles and quadrangles of 30 pixels width in average) is adjusted on the image, see Figure 3.

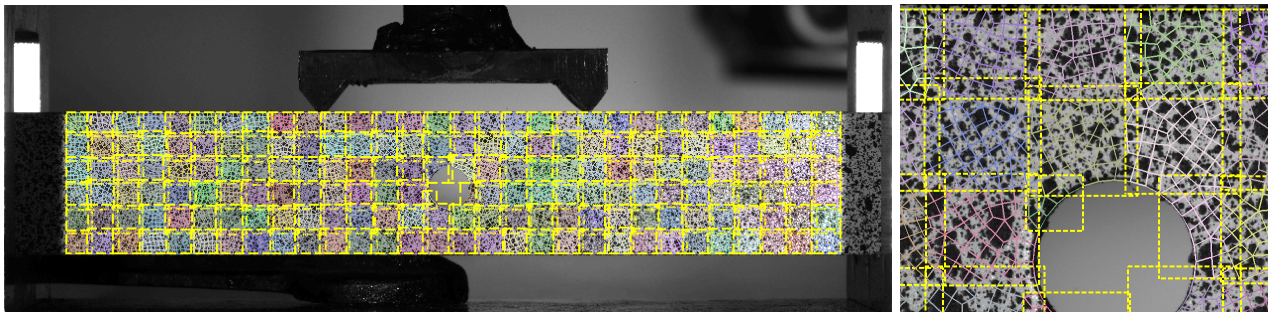

Figure 3: Example of a four point bending test. Image and domain decomposition in the case of 179 subdomains. The overlapping subset images f_s are in yellow dashed line. The finite elements belonging to a same subdomain are plotted with the same color. A zoom is provided on the right.

3.2 Initialisation and DD solution

A first decomposition into 179 subdomains[1] is considered (Fig. 3). The average subdomain size is 160 pixels. The analysis is performed with a stopping tolerance for correlation and CG iterations of 10^{-3}. First, the initialisation is performed on each subdomain independantly. This stage is highly parallelisable since no communications are required between subdomains. This initial displacement solution is plotted in Figure 4 (top) with an amplification factor of 50. The colorscale corresponds to the horizontal component of the displacement field.

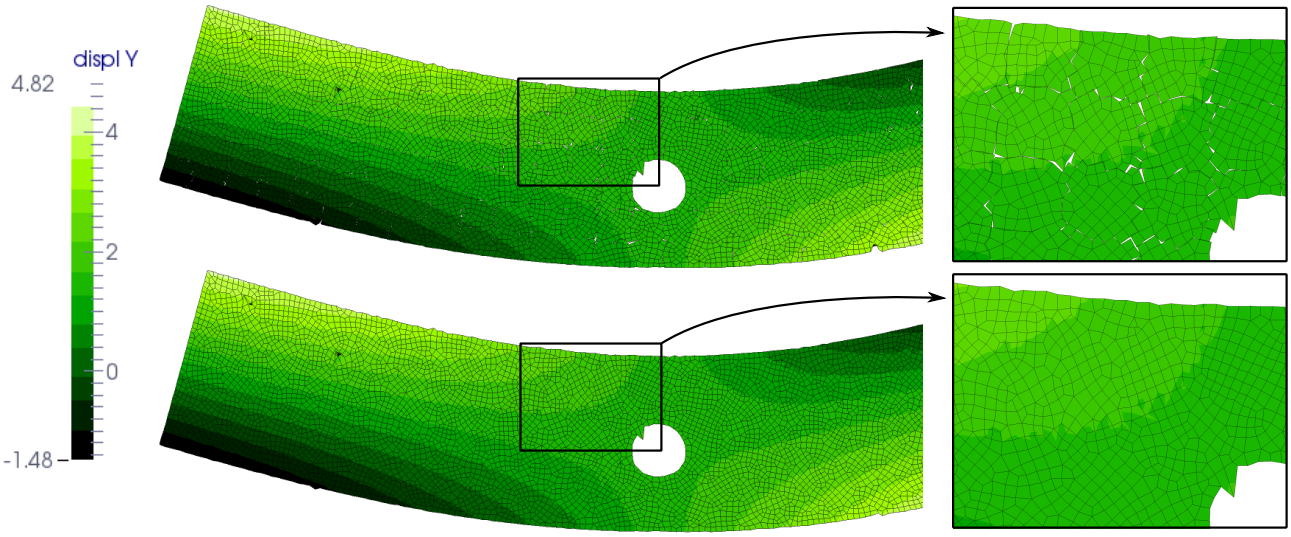

Figure 4: Example of a four point bending test: displacement solution in pixels (amplification factor 50): (top) FE-DIC solution computed independently on each subdomain (bloc *Initialis.* in Figure 2) and (bottom) continuous solution computed by the domain decomposition method (bloc *Correlation iterations* in Figure 2)

It can be noticed that this low-cost solution is a good initialisation for the proposed domain decomposition solver. A zoom in the top right is provided to show that the displacement continuity is actually not verified between subdomains. It seems clear that the extra effort, provided by the domain decomposition solver, to make the displacement continuous between subdomains, is rather slight. In this case, it took 8 extra iterations to converge. The resulting displacement is plotted in Figure 3 (bottom). The zoom on the bottom right shows that the displacement is then continuous.

[1] Ω is devided into 180 (6×30) regions. But no subdomain is associated to the region of the hole since it is not meshed.

3.3 Convergence acceleration

The variation of the norm of the residual $\mathbf{r}_i$ as a function of the CG iteration i for the third correlation iteration ($k = 3$) is plotted in Figure 5 for the five following solvers:

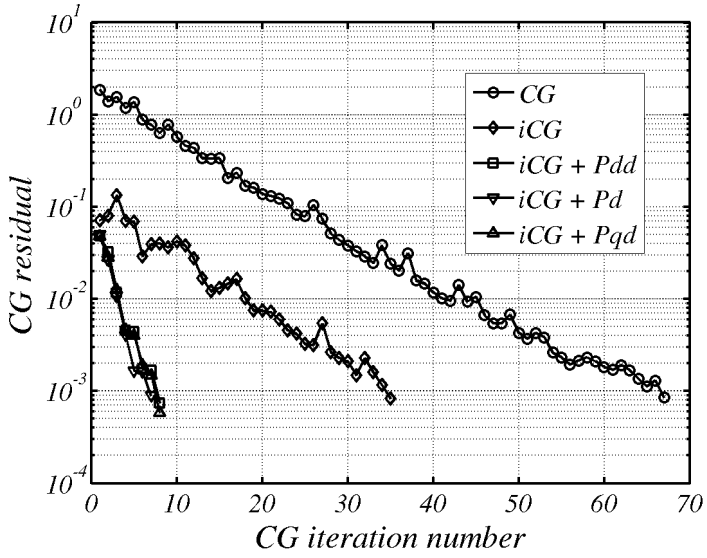

Figure 5: Variation of the norm of the residual $\mathbf{r}_i$ as a function of the iteration number i for the third correlation iteration $k = 3$ as a function of the choosen solver

- **CG**. A standard conjuguate gradient without preconditionning ($\mathbf{P}$ set to identity) initialised by $\mathbf{\Lambda}_0 = 0$ at each correlation iteration k.
- **iCG**. A standard conjuguate gradient without preconditionning ($\mathbf{P}$ set to identity) where the solution $\mathbf{\Lambda}$ of the previous correlation iteration $(k-1)$ is used to initialize the CG at correlation iteration k.
- **iCG Pdd**. The same as **iCG** but with the double diagonal preconditionner $\mathbf{P}_{dd}$.
- **iCG Pd**. The same as **iCG** but with the diagonal preconditionner $\mathbf{P}_{d}$.
- **iCG Pqd**. The same as **iCG** but with the quasi diagonal preconditionner $\mathbf{P}_{qd}$.

It took around 65 iterations for the classic CG to reach convergence. By merely initializing the CG with the previous solution vector $\mathbf{\Lambda}$, it can be seen that the number of iterations is almost divided by two since the initial estimate of $\mathbf{\Lambda}$ is better by one decade in comparison to $\mathbf{\Lambda} = 0$. However, this technique is not actually an acceleration technique since the convergence rate is the same than without initialisation. When using the proposed preconditionners, it can be noticed that the convergence rate itself is also improved.

The number of iterations required by the CG to reach the convergence criterion is reported in Figure 6 as a function of the chosen solver for the eight correlation iterations. The total number of CG iteration used by the domain decomposition solver can be drastically reduced when using both initialisation and preconditionning. According to this example, all of the three proposed preconditionners are efficient in reducing the number of iterations. The quasi-diagonal preconditionner seems the more efficient in this case.

In order to illustrate the sparsity of the quasi-diagonal preconditionner, the non-zero values of $\mathbf{P}_{qd}$ are potted in black in Figure 7 (left). The matrix is actually tridiagonal, but the number of non-zero extra diagonal elements is very low. It is equal to 2×568 (by symmetry) whereas the number interface dof is 5238. It seems that $\mathbf{P}_{qd}$ is a cheap but rather good approximation of the dual Schur complement $\mathbf{S}^d$ even if the latter is not banded at all. Indeed, its non-zero values are plotted in Figure 7 (right) for comparison purposes.

3.4 Metrological and computational performances

The measurement uncertainty is finally analysed in Figure 8. As mentionned above, the domain decomposition method actually converges toward the monolithic solution (one single domain). Therefore, the metrological performances are the same. However, an *a priori* performance analysis is carried out in order to illustrate the effect of bonding the subdomains on measurement uncertainties. The standard displacement uncertainty is

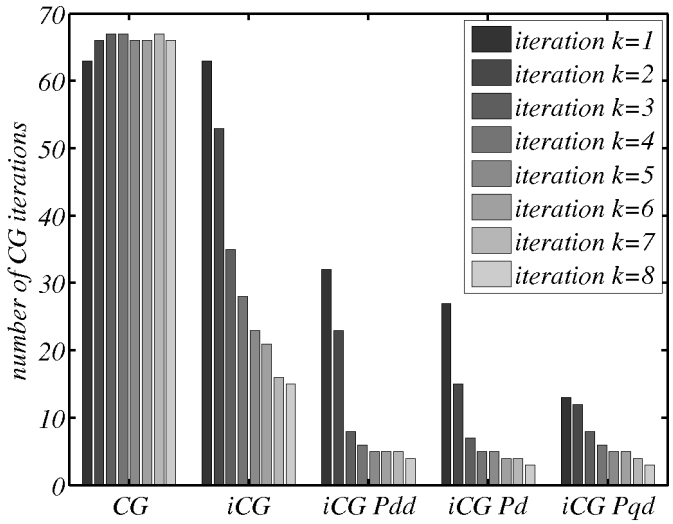

Figure 6: Number of iteration required to satisfy the convergence indicator as a function of the correlation iteration k for 5 different solvers.

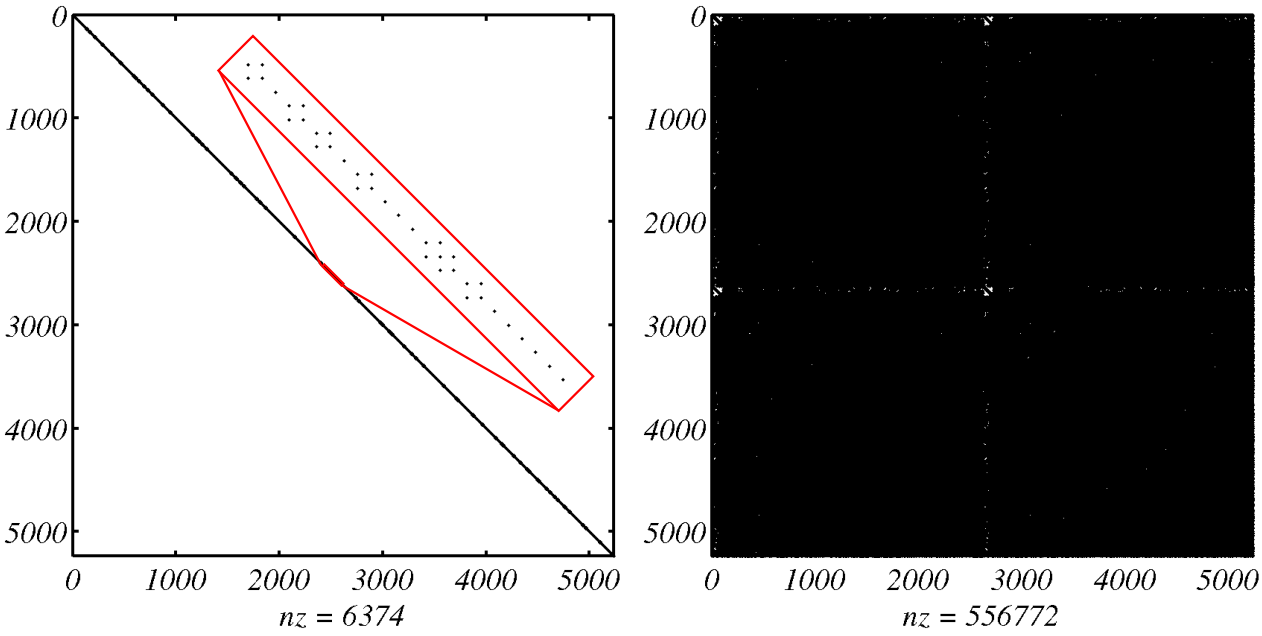

Figure 7: Non-zero elements of the quasi-diagonal preconditionner $\mathbf{P}_{qd}$ (left) and comparison to those of the dual Schur complement $\mathbf{S}^d$ (right).

estimated by subjecting the reference image to a sub-pixel rigid body shift with a Fast Fourier Transform [5]. Then the measurement is performed between the reference and shifted images. The standard deviation of the error between measured and prescribed displacement is plotted as a function of the average subdomain size in pixels. This standard uncertainty is estimated for the initial displacement estimate (*uncoupled subdomains*), the solution to the proposed domain decomposition solver (*coupled subdomains*) and a standard single domain FE-DIC method used as a reference. As expected, the uncertainty of the solution to the domain decomposition solver is equal to the one with a single subdomain solution, regardless of the subdomains size. On the other hand, the solution computed independently on each subdomain (which is used as initialisation), is subject to larger uncertainties, as subset-based DIC methods do [17], since continuity is not prescribed between subdomains.

At this stage, only a sequential implementation of the method was performed in Matlab. It is subsequently not possible to provide a relevant estimate of the speed-up. However, the average normalised CPU time required to compute one iteration of local FE-DIC (including image interpolation and FE system resolution) is plotted

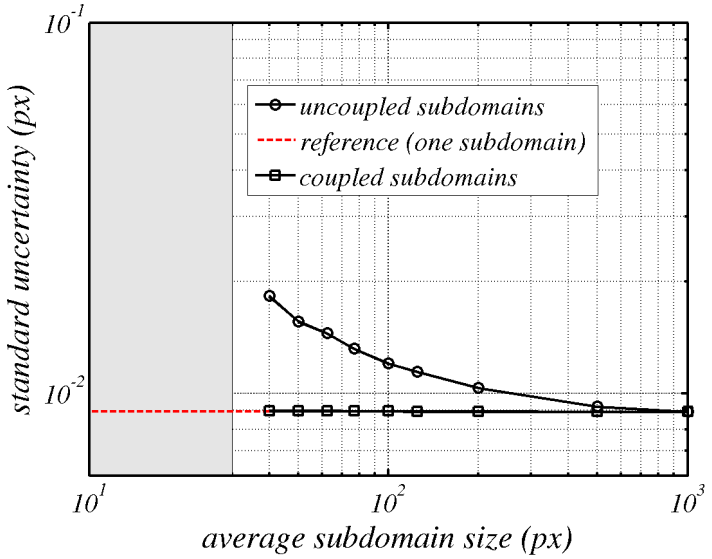

Figure 8: A priori performance analysis: Variation of the standard displacement uncertainty with respect to graylevel interpolation for the initial displacement estimate (*uncoupled subdomains*), the solution to the domain decomposition solver (*coupled subdomains*) and a standard single domain FE-DIC method (red dashed line). The gray zone corresponds to subdomain size smaller than the average element size of the mesh.

in Figure 9 versus average sudomain size. It appears that the numerical complexity seems to be a bit less

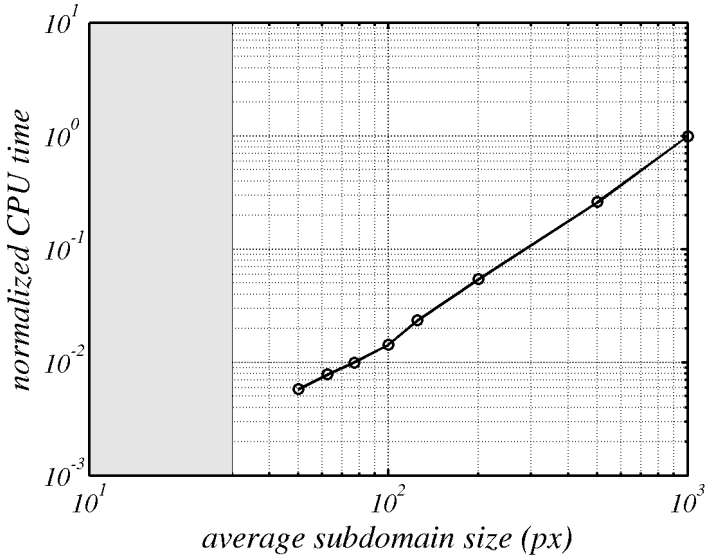

Figure 9: Insight in CPU performance: average CPU time required to compute one iteration of local FE-DIC normalised by the cost of one iteration of the global FE-DIC problem.

that $O(N^2)$. In other words, the CPU time of one iteration is divided by almost 100 when the size of the subdomains is divided by 10. With a sequential implementation of the method, 65% of the CPU time is devoted to compute the initialisation (first bloc of Figure 2), whereas the remaining 35% are used to perform the 8 extra iterations with the DD solver (second bloc of Figure 2). Since the first 65% correspond to computations that are independent by subdomain (it requires no data exchange between subdomains), this first initialisation is thus highly parallelizable and its computational cost, with a parallel implementation, is expected to be divided by the number of subdomains. The second part (35%) is also highly parallelizable, but requires some data exchange between subdomains. The results presented in Figures 8 and 9 exemplify that the proposed approach combines the advantages of FE-based DIC and subset-based DIC methods.

4 Summary and perspectives

A non-overlapping dual domain decomposition method is proposed for finite element based digital image correlation. It consists in splitting the resolution of a global FE-DIC problem into a set of local FE-DIC sub-problems, based on smaller independent submeshes and subset images. The initial problem is condensed on the interface. A well initialised conjuguate gradient solver combined with three possible cheap preconditionners is presented. The method is used to analyse a 2D DIC problem with real high resolution images. The fact that the method has the same metrological performances as a classic FE-DIC method is illustrated. The first CPU estimations gives a glimpse of the potential of a parallel implementation of the method. It should offer the scalability of subset-based methods to global approaches to DIC. The use of such a domain decomposition method should be of great interest for the correlation of high definition digital volume images that are out of reach with standard FE DVC approaches [24, 22].

Essentially developed for high performance computing considerations, such a method may have also other applications. Indeed, this partitionning method is also a good candidate for measuring continuous displacements in the case of a multiple-camera instrumentation of a single specimen [31, 32]. This kind of instrumentation yields, in essence, a set of independent images, that the proposed domain decomposition method would manage conveniently and efficiently. The extention to stereo digital image correlation could subsequently be a good candidate for measurements on large structures. This will also be a good tool for the high resolution analysis of complex microstructures present, for instance, in composite materials, polycrystaline metals or biomaterials [29, 25, 13]. Such a coupling method could also be used to couple finite elements with other interpolations types, like, for instance, X-FEM [38] and Williams' series expansions [41], for the estimation of stress intensity factors of curvilinear cracks, following what is done in simulation [36].

References

[1] B.K. Bay, T.S. Smith, D.P. Fyhrie, and M. Saad. Digital volume correlation: three-dimensional strain mapping using x-ray tomography. *Experimental Mechanics*, 39(3):217–226, 1999.

[2] T. Belytschko, W.K. Liu, and B. Moran. *Nonlinear Finite Elements for Continua and Structures*. John Wiley & Sons, New York, 2000.

[3] G. Besnard, F. Hild, and S. Roux. finite-element displacement fields analysis from digital images: Application to Portevin-le Châtelier bands. *Experimental Mechanics*, 46(6):789–803, 2006.

[4] B. Blaysat, J.P.M. Hoefnagels, G. Lubineau, M. Alfano, and M.G.D. Geers. Interface debonding characterization by image correlation integrated with double cantilever beam kinematics. *International Journal of Solids and Structures*, page Online first, 2014.

[5] M. Bornert, F. Brémand, P. Doumalin, J.-C. Dupré, M. Fazzini, M. Grédiac, F. Hild, S. Mistou, J. Molimard, J.-J. Orteu, L. Robert, Y. Surrel, P. Vacher, and B. Wattrisse. Assessment of digital image correlation measurement errors: methodology and results. *Experimental Mechanics*, 49(3):353–370, june 2009.

[6] P. Cheng, M. Sutton, H.W. Schreier, and S. R. McNeill. Full-field speckle pattern image correlation with b-spline deformation function. *Experimental mechanics*, 42(3):344–352, 2002.

[7] J.E. Dufour, F. Hild, and S. Roux. Integrated digital image correlation for the evaluation and correction of optical distortions. *Opt. Lasers Eng.*, 56:121–133, 2014.

[8] T. Elguedj, J. Réthoré, and A. Buteri. Isogeometric analysis for strain field measurements. *Computer Methods in Applied Mechanics and Engineering*, 200(1-4):40–56, 2010.

[9] C. Farhat and F.X. Roux. A method of finite element tearing and interconnecting and its parallel solution algorithm. *International Journal for Numerical Methods in Engineering*, 32:1205–1227, 1991.

[10] R. Fedele, L. Galantucci, and A. Ciani. Global 2D digital image correlation for motion estimation in a finite element framework: a variational formulation and a regularized, pyramidal, multi-grid implementation. *International Journal for Numerical Methods in Engineering*, 96(12):739–762, 2013.

[11] J. Fehrenbach and M. Masmoudi. A fast algorithm for image registration. *Comptes Rendus Mathématique*, 346(9-10):593–598, 2008.

[12] R. Glowinski, G.H. Golub, G.A. Meurant, and J. Périaux. *First International Symposium on Domain Decomposition Methods for Partial Differential Equations*. SIAM, Philadelphia, PA, USA, 1988.

[13] L.A. Gomes Perini, J.-C. Passieux, and J.-N. Périé. A multigrid PGD-based algorithm for volumetric displacement fields measurements. *Strain*, 50(4):355–367, 2014.

[14] P. Gosselet and C. Rey. Non-overlapping domain decomposition methods in structural mechanics. *Archives of Computational Methods in Engineering*, 13:515–572, 2006.

[15] P. Gosselet, C. Rey, and J. Pebrel. Total and selective reuse of Krylov subspaces for the resolution of sequences of nonlinear structural problems. *International Journal for Numerical Methods in Engineering*, 94(1):60–83, 2013.

[16] F. Hild and S. Roux. Measuring stress intensity factors with a camera: Integrated digital image correlation (I-DIC). *Comptes Rendus Mécanique*, 334(1):8–12, 2006.

[17] F. Hild and S. Roux. Comparison of local and global approaches to digital image correlation. *Experimental Mechanics*, 52(9):1503–1519, 2012.

[18] F. Hild, S. Roux, N. Guerrero, M.E. Marante, and J. Flórez-López. Calibration of constitutive models of steel beams subject to local buckling by using digital image correlation. *European Journal of Mechanics - A/Solids*, 30(1):1 – 10, 2011.

[19] B.K.P. Horn and G. Schunck. Determining optical flow. *Artificial Intelligence*, 17:185–203, 1981.

[20] P. Kerfriden, O. Allix, and P. Gosselet. A three-scale domain decomposition method for the 3D analysis of debonding in laminates. *Computational mechanics*, 44(3):343–362, 2009.

[21] P. Ladevèze. *Nonlinear computationnal structural mechanics–New approaches and non-incremental methods of calculation*. Springer Verlag, 1999.

[22] H. Leclerc, J.-N. Périé, F. Hild, and S. Roux. Digital volume correlation: What are the limits to the spatial resolution? *Mechanics & Industry*, 13(6):361–371, november 2012.

[23] H. Leclerc, J.-N. Périé, S. Roux, and F. Hild. Integrated digital image correlation for the identification of mechanical properties. *Lectures Notes in Computer Sciences*, 5496:161–171, 2009.

[24] H. Leclerc, J.-N. Périé, S. Roux, and F. Hild. Voxel-scale digital volume correlation. *Experimental Mechanics*, 51(4):479–490, 2011.

[25] P. Lecomte-Grosbras, J. Réthoré, N. Limodin, J.-F. Witz, and M. Brieu. Three-dimensional investigation of free-edge effects in laminate composites using x-ray tomography and digital volume correlation. *Experimental Mechanics*, 2014.

[26] B.D. Lucas and T. Kanade. An iterative image registration technique with an application to stereo vision. In *Proceedings of Imaging Understanding Workshop*, pages 121–130, 1981.

[27] P. F. Luo, Y. J. Chao, M. A. Sutton, and W. H. Peters. Accurate measurement of three-dimensional deformations in deformable and rigid bodies using computer vision. *Experimental Mechanics*, 33(2):123–132, 1993.

[28] J. Mandel. Balancing domain decomposition. *Communications in Numerical Methods in Engineering*, 9:233–241, 1993.

[29] F. Mortazavi, E. Ghossein, M. Lvesque, and I. Villemure. High resolution measurement of internal full-field displacements and strains using global spectral digital volume correlation. *Optics and Lasers in Engineering*, 55:44–52, 2014.

[30] F Mortazavi, M Levesque, and I Villemure. Image-based continuous displacement measurements using an improved spectral approach. *Strain*, 49(3):233–248, 2013.

[31] J.-J. Orteu, F. Bugarin, J. Harvent, L. Robert, and V. Velay. Multiple-camera instrumentation of a single point incremental forming process pilot for shape and 3D displacement measurements: Methodology and results. *Experimental Mechanics*, 51(4):625–639, april 2011.

[32] J.-C. Passieux, F. Bugarin, C. David, J.-N. Périé, and L. Robert. Multiscale displacement field measurement using digital image correlation: Application to the identification of elastic properties. *Experimental Mechanics*, 10.1007/s11340-014-9872-4:In press, 2014.

[33] J.-C. Passieux, P. Ladevèze, and D. Néron. A scalable time-space multiscale domain decomposition method: adaptive time scale separation. *Comput. Mech.*, 46(4):621–633, 2010.

[34] J.-C. Passieux, P. Navarro, J.-N. Périé, S. Marguet, and J.-F. Ferrero. A digital image correlation method for tracking planar motions of rigid spheres: application to medium velocity impacts. *Experimental Mechanics*, 54(8):1453–1466, 2014.

[35] J.-C. Passieux and J.-N. Périé. High resolution digital image correlation using Proper Generalized Decomposition: PGD-DIC. *International Journal for Numerical Methods in Engineering*, 92(6):531–550, 2012.

[36] J.-C. Passieux, J. Réthoré, A. Gravouil, and M.-C. Baietto. Local/global non-intrusive crack propagation simulation using a multigrid X-FEM solver. *Computational Mechanics*, 56(2):1381–1393, 2013.

[37] J. Rannou, N. Limodin, J. Réthoré, A. Gravouil, W. Ludwig, M.-C. Baietto-Dubourg, J.-Y. Buffiére, A. Combescure, F. Hild, and S. Roux. Three dimensional experimental and numerical multiscale analysis of a fatigue crack. *Computer Methods in Applied Mechanics and Engineering*, 199:1307–1325, 2010.

[38] J. Réthoré, F. Hild, and S. Roux. Shear-band capturing using a multiscale extended digital image correlation technique. *Computer Methods in Applied Mechanics and Engineering*, 196(49-52):5016–5030, 2007.

[39] J. Réthoré, F. Morestin, L. Lafarge, and P. Valverde. 3D displacement measurements using a single camera. *Optics and Lasers in Engineering*, 57(0):20 – 27, 2014.

[40] J. Réthoré, S. Roux, and F. Hild. From pictures to extended finite elements: extended digital image correlation (X-DIC). *Comptes Rendus Mécanique*, 335(3):131 – 137, 2007.

[41] S. Roux and F. Hild. Stress intensity factor measurements from digital image correlation: post-processing and integrated approaches. *Int J. Fract*, 140:141–157, 2006.

[42] S. Roux, F. Hild, and Y. Berthaud. Correlation image velocimetry : a spectral approach. *Applied Optics*, 41(108–115), 2002.

[43] S. Roux, J. Réthoré, and F. Hild. Digital image correlation and fracture: an advanced technique for estimating stress intensity factors of 2D and 3D cracks. *J. Phys. D: Appl. Phys.*, 42(214004), 2009.

[44] Y. Sun, J.H.L. Pang, C. Khuen Wong, and F. Su. Finite element formulation for a digital image correlation method. *Applied Optics*, 44(34):7357–7363, 2005.

[45] M.A. Sutton, J.-J. Orteu, and H. Schreier. *Image correlation for shape, motion and deformation measurements: Basic Concepts, Theory and Applications*. Springer, New York, NY (USA), 2009.

[46] M.A. Sutton, W.J. Wolters, W.H. Peters, W.F. Ranson, and S.R. McNeill. Determination of displacements using an improved digital correlation method. *Image and Vision Computing*, 1(3):133–139, 1983.